THE COSMIC HORSESHOE: DISCOVERY OF AN EINSTEIN RING AROUND A GIANT LUMINOUS RED GALAXY

V. Belokurov[1], N. W. Evans[1], A. Moiseev[2], L. J. King[1], P. C. Hewett[1], M. Pettini[1], L. Wyrzykowski[1,4],
R. G. McMahon[1], M. C. Smith[1], G. Gilmore[1], S. F. Sanchez[3], A. Udalski[4], S. Koposov[5], D. B. Zucker[1],
C. J. Walcher[6]

ABSTRACT

We report the discovery of an almost complete ($\sim 300°$) Einstein ring of diameter $10''$ in Sloan Digital Sky Survey (SDSS) Data Release 5 (DR5). Spectroscopic data from the 6m telescope of the Special Astrophysical Observatory reveals that the deflecting galaxy has a line-of-sight velocity dispersion in excess of 400 kms^{-1} and a redshift of 0.444, whilst the source is a star-forming galaxy with a redshift of 2.379. From its color, luminosity and velocity dispersion, we argue that this is the most massive galaxy lens hitherto discovered.

Subject headings: gravitational lensing – galaxies: structure – galaxies: evolution

1. INTRODUCTION

There have been many optical giant arcs discovered, caused by the lensing effects of massive galaxy clusters and their central galaxies. But, few optical rings have ever been found, despite theoretical predictions that they should be abundant (Miralda-Escude & Lehar 1992). Warren et al. (1996) found 0047-2808, which is a high redshift star-forming galaxy lensed by a massive early-type galaxy into a partial ($\sim 170°$) Einstein ring of 2″.70 diameter, while King et al. (1998) discovered a complete Einstein ring in the near-infrared around B1938+666. Cabanac et al. (2005) found a nearly complete ($\sim 260°$) Einstein ring of diameter 2″.96 produced by the lensing of a starburst galaxy by a massive and isolated elliptical galaxy. The Sloan Lens ACS Survey (SLACS, Bolton et al. 2006) has also identified a number of partial optical rings, based on the identification of anomalous emission lines in Sloan Digital Sky Survey (SDSS) spectra together with confirmatory follow-up from the Advanced Camera for Surveys. Here, we report the discovery of the Cosmic Horseshoe – an almost complete ($\sim 300°$), giant Einstein ring, with a diameter of $\sim 10''$ in SDSS data. Throughout the paper, we use the standard cosmology $\Omega_{\rm m} = 0.3$, $\Omega_{\Lambda} = 0.7$, $H_0 = 70$ km s^{-1} Mpc^{-1}.

2. DISCOVERY AND FOLLOW-UP

Previous search strategies with SDSS data can be divided into three kinds. The first discovery was made by Inada et al. (2003a), who searched around spectroscopically identified quasars looking for stellar-like objects with a similar color to provide candidates for follow-up, and found the spectacular 14″.62 separation lens SDSS
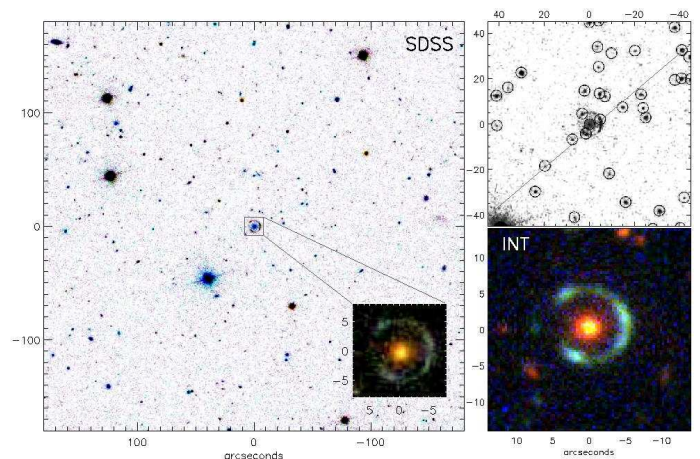

FIG. 1.— Left: SDSS view of the sky composed from g, r, i images around the Cosmic Horseshoe. Most of the objects in the field are faint galaxies. The inset shows $16'' \times 16''$ cut-out centered on the lens. Note the bluish color of the ring. Top right: SDSS g, r, i composite with objects detected by the SDSS pipeline marked with circles. We also show the slit position for SAO follow-up. Bottom right: INT u, g, i composite from follow-up data.

J1004+4112. The remaining two methods target smaller separation lenses, in which the images are unresolved by SDSS. Inada et al. (2003b) and Johnston et al. (2003) searched through spectroscopically identified quasars, looking for evidence of extended sources corresponding to unresolved, multiple images. The most widely-used strategy is to search through the spectroscopic database looking for emission lines of high redshift objects within the spectrum of lower redshift early-type galaxies (Willis et al. 2005; Bolton et al. 2006). Here, we introduce a new method, inspired by the recent, serendipitous discovery of the 8 O'clock Arc, which is a Lyman Break galaxy lensed into three images merging into an extended arc (Allam et al. 2006). The SDSS pipeline resolved the arc into three objects. This suggests searching for multiple, blue, faint companions around luminous red galaxies (LRGs) in the SDSS object catalogue. The search is fast, so it is easy to experiment with different magnitude and color cuts, as well as search radii.

[1] Institute of Astronomy, University of Cambridge, Madingley Road, Cambridge CB3 0HA, UK; vasily,nwe@ast.cam.ac.uk
[2] Special Astrophysical Observatory, Nizhniy Arkhyz, Karachaevo-Cherkessiya, Russia; moisav@sao.ru
[3] CAHA de Calar Alto (CSIC-MPIA), E4004 Almera, Spain
[4] Warsaw University Observatory, Al. Ujazdowskie 4, 00-479, Poland
[5] MPIA, Königstuhl 17, 69117 Heidelberg, Germany
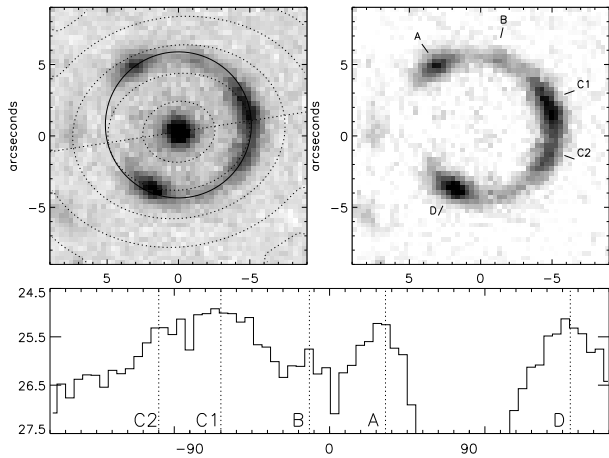[6] CNRS-Université de Provence, BP8, 13376 Marseille Cedex 12, France

FIG. 2.— Left: g band INT images of a $18'' \times 18''$ field of view centered on the Cosmic Horseshoe. Dotted lines mark the major axis of the LRG and contours show isophotes at 1,2,3,4,5 R_{eff} along the major axis. The best fit circle through the ring is shown as a solid line. Right: Decomposition of the light into the ring after subtraction of the luminosity model for the LRG. Also shown is the profile along the ring in the inset. The locations of the four maxima are marked.

For example, selecting lenses in DR5 to be brighter than $r = 19.5$ and $g-r > 0.6$, together with sources within $6''$ that are fainter than $r = 19.5$ and bluer than $g-r = 0.5$ yields 3 very strong candidates. One of the three candidates is the 8 O'clock arc – another is the subject of this *Letter*, the Cosmic Horseshoe.

The left panel of Fig. 1 shows a g, r, i composite image. Most of the faint objects in the field of view are galaxies, but the environment is clearly not that of a rich cluster. The inset shows a $16'' \times 16''$ cut-out, in which the central lens galaxy is surrounded by a $\sim 300°$ ring of radius $\sim 5''$. This makes it the largest, and one of the most complete, optical rings ever discovered.

We obtained imaging follow-up data at the 2.5m *Isaac Newton Telescope* (INT), La Palma and spectroscopy at the 6m BTA telescope of the *Special Astrophysical Observatory* (SAO), Nizhnij Arkhyz, Russia. Observations were carried on the INT on the night (UT) of 2007 May 12 with the Wide Field Camera (WFC). The exposure times were 600 s in each of the three wavebands u, g and i – which are similar to the SDSS filters. The measured seeing (FWHM) on the images ($0.33''$ pixels) was $1.30''$, $1.26''$ and $1.21''$ in u, g and i respectively. The INT data are roughly a magnitude deeper than the SDSS data and were reduced using the CASU INT WFC pipeline toolkit (Irwin & Lewis 2001). The bottom right panel of Fig. 1 shows the u, g, i composite field of view of $24'' \times 24''$ centered on the lens galaxy. The Cosmic Horseshoe is shown with great clarity in the panels of Fig 2. We can extract the properties of the LRG, such as magnitude, effective radius, ellipticity and orientation, by masking out the ring emission and fitting a PSF-convolved de Vaucouleurs profile as listed in Table 1. Our INT magnitudes agree with the SDSS magnitudes reported in the Table, although SDSS overestimates the g band effective radius because of contamination from the ring. The shape of the isophotes of the LRG is shown in dotted lines. In the right panel, the light from the lens galaxy is subtracted to leave a clearer picture of the ring in the g band. The

surface brightness profile along the ring in magnitudes arcsec^{-2} is shown in the inset. There are four maxima, A, B, C and D, whose right ascension and declination offsets from the LRG are: A : $(3''.0, 4''.6)$, B : $(-1''.1, 5''.2)$, C : $(-4''.7, 2''.2)$ and D : $(2''.0, -4''.0)$ together with errors of $\lesssim 0''.4$. There is some evidence that C may even be considered as two merging images at C_1 $(-4''.7, 2''.2)$ and C_2 $(-4''.8, -1''.7)$. Fig 3 shows the number density of galaxies with photometric redshifts provided by SDSS in the range $0.35 < z < 0.55$. In the left panel, a large-scale filamentary structure can be discerned. The middle panel shows that the Cosmic Horseshoe lies in a group of galaxies – the enhancement in number density over the background is ~ 6. The lens is the brightest object in the group of ~ 26 members, as is clear from the cumulative luminosity function in the right panel.

Long-slit spectral observations were performed on 2007 May 15/16 with the multi-mode focal reducer SCORPIO (Afanasiev & Moiseev 2005) installed at the prime focus of the BTA 6-m telescope at the SAO. The seeing was $1''.7$. A $1''.0$ wide slit was placed to intercept the two brighter arcs in the ring (C and D in Fig. 2) and to include some of the light from the lens galaxy, as shown in the top right panel of Fig. 1. We used the VPHG550G grism which covers the wavelength interval 3650–7550 Å with a spectral resolution 8-10 Å FWHM. With a CCD EEV 42-40 2k $\times$ 2k detector, the reciprocal dispersion was 1.9 Å per pixel. The total exposure time was 3600 s, divided into six 10-minute exposures. The target was moved along the slit between exposures to ease background subtraction and CCD fringes removal in the data processing. The bias subtraction, geometrical corrections, flat fielding, sky subtraction, and calibration to flux units (F_λ) was performed by means of IDL-based software.

The top panel of Fig. 4 shows a cut-out of the two-dimensional spectrum with position along the slit plotted against the dispersion. The slit also passes through a nearby star, which causes the spectrum in the topmost pixels. In the lower part, the blue spectrum is dominated by two images of the source, whilst the red spectrum by the lensing galaxy. The lower panels show extracted one-dimensional spectra. The middle one is the sum of the two source images; there is a strong narrow line which is Ly α emission, together with accompanying Ly α forest bluewards and multiple absorption lines redwards. This yields a measurement of the source redshift as $z = 2.379$. The lower panel is the lens galaxy spectrum, which shows the characteristic features of a LRG. The lens redshift is $z = 0.444$. Although Ca H and K absorption is detected in the lensing galaxy spectrum, the signal-to-noise (S/N) ratio is modest, ~ 10, and the resolution relatively low. However, the inset in the lower panel shows the instrumental resolution and the Ca H and K lines, which are clearly resolved. Performing fits of Gaussian line profiles to the absorption produces a velocity dispersion estimate of $430 \pm 50 \, \mathrm{km s^{-1}}$, where the principal uncertainty arises from the placement of the 'continuum'. The spectrograph slit was not aligned across the centre of the galaxy but, given the relatively poor seeing, the spectrum is dominated by light from within the half-light radius of the galaxy.
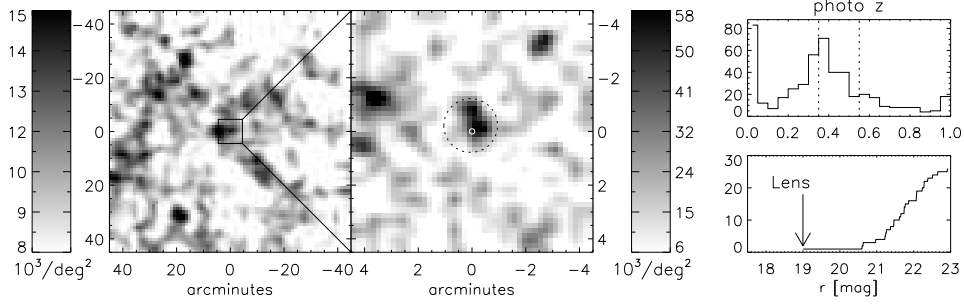
3. DISCUSSION

FIG. 3.— Density of galaxies in the vicinity of the object with SDSS photometric redshifts in the range $0.35 < z < 0.55$. Left: Large scale structure. Middle: Zoom-in on the lens marked by white ring, shown to scale. The lens belongs to the group of ~ 26 galaxies, marked by dashed circle of $1'$ radius. Right: Redshift distribution (upper panel) for all galaxies in the $9' \times 9'$ box. For galaxies in the range $0.35 < z < 0.55$ (dashed lines), we build the r-band cumulative LF of the group members (lower panel). The lens is the brightest galaxy in the group, most of the other members are fainter than $21^{\mathrm{m}}5$.
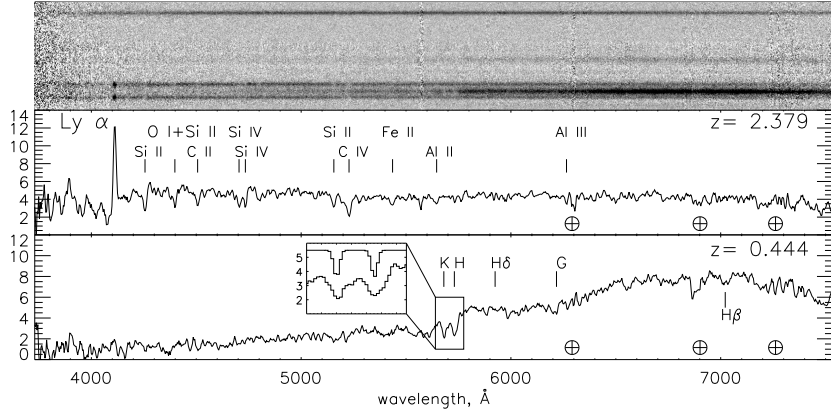
FIG. 4.— Top: Cutout of the SCORPIO 2D spectrum, the horizontal coordinate is the dispersion, the vertical coordinate is the location on the slit. In the lower part, 2 ring images are clearly visible at short wavelength (note the bright Lyα blobs) with the lens appearing at longer wavelengths. Middle: Sum of two extracted 1D image spectra with absorption lines from Table 1 of Shapley et al. (2003). Bottom: 1D lens spectrum with Ca H and K lines marked. As a demonstration that the lines are resolved, we show in the inset a zoom of the H and K lines (lower) and the instrumental resolution (upper). Note the prominent atmospheric absorption marked by $\oplus$ symbols. The spectra are shown in flux units of 10^{-18} erg s^{-1} cm^{-2} $\mathring{A}^{-1}$.
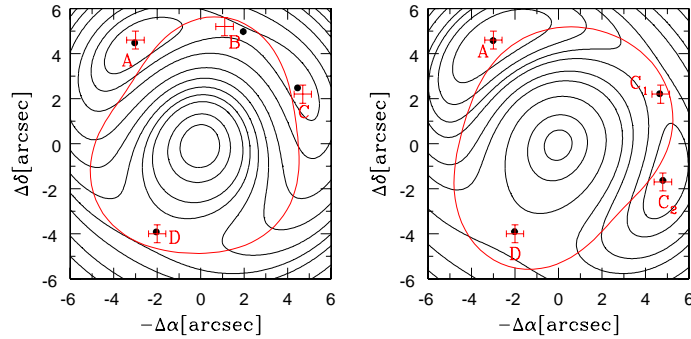

FIG. 5.— Contours of the Fermat time delay surface for two possible lens models of Cosmic Horseshoe, together with the locations of the stationary points which mark the predicted image positions. The critical curve of the lens model, which is also a contour of constant convergence, is shown in red, together with the observed image locations. Left: The model uses eqn. (5) of Evans & Witt (2003) with the Fourier coefficients ($a_0 = 9.89$, $a_2 = 0.090$, $b_2 = -0.11$, $a_3 = 0.02$, $b_3 = -0.04$) to reproduce image locations A,B, C and D. Right: A similar model, but with Fourier coefficients ($a_0 = 10.07$, $a_2 = 0.066$, $b_2 = -0.22$, $a_3 = -0.03$, $b_3 = -0.01$) to reproduce image locations A, C_1, C_2 and D.

3.1. Source

The spectrum in Fig. 4 shows the source is a star-forming galaxy at $z = 2.379$. From the observed wavelengths of the ten labelled absorption lines, we deduce a mean redshift $\langle z_{abs} \rangle = 2.3767 \pm 0.0006$, while the peak of the Lyα emission line gives $z_{em} \simeq 2.3824$. The overall character of the spectrum is typical of BX galaxies in the surveys by Steidel et al. (2004). These are galaxies at a mean redshift $\langle z \rangle \simeq 2.2$ selected from their blue rest-frame UV colours. In finer detail, the spectrum resembles most closely the subset of these galaxies which are relatively young, with assembled stellar masses $\langle M^* \rangle \simeq 5 \times 10^9 M_\odot$ and metallicities of about 1/3 solar. The composite spectrum of galaxies with these characteristics has been discussed by Erb et al. (2006a) and has typical rest-frame equivalent widths of the interstellar lines $W_{IS} \simeq 1.5 - 2$ Å, and a similar strength of the Ly α emission line. The closest local analogue is the field spectrum of nearby starburst galaxies (Chandar et al. 2005). The difference between Lyα emission and interstellar absorption redshifts found here is typical of high redshift star-forming galaxies and is generally interpreted as resulting from large-scale outflows of the interstellar medium in galaxies with high rates of star formation, driven by kinetic energy deposited by massive star winds and supernovae. Adopting the median blueshift of 165 km s^{-1} of the interstellar absorption lines relative to the H II regions producing Hα emission (Steidel et al. 2007, in preparation), we deduce a systemic redshift of $z_{sys} = 2.379$.

The galaxy appears to be of fiducial luminosity. Interpolating between the measured g and i magnitudes in Table 1, we deduce an absolute magnitude at 1700 Å $AB_{1700} = -25.4$ in the standard cosmology. If the magnification factor is ~ 35 (see next Section), or 3.9 mag, this corresponds to an intrinsic $AB_{1700} = -21.5$, or $L \simeq 1.6L^*$, according to the recent determination of the luminosity function of BX galaxies by Reddy et al. (2007). The colours of the lensed galaxy are typical of those of most BX galaxies. The $u-g$ and $g-i$ colours indicated by the photometry in Table 1 imply a UV spectral slope redder than the essentially flat spectrum ($F_\nu \propto \nu^0$) expected for an unobscured star-forming galaxy (e.g. Leitherer et al. 1999). Assuming that the Calzetti et al. (2000) obscuration law applies, we deduce $E(B-V) = 0.2$, close to the median of the distribution of the values reported by Erb et al. (2006b) for BX galaxies. The corresponding attenuation at 1700 Å is a factor of ~ 6.

3.2. Lens

Bernardi et al. (2006) found 70 galaxies with dispersions > 350 kms^{-1} that were not superpositions in the spectroscopic part of the SDSS DR1. These are the galaxies with largest velocity dispersions and might harbour the most massive black holes. The fact that the PSF-convolved de Vaucouleurs model gives an excellent fit to the light distribution of the lens galaxy minimises the chance that the high velocity dispersion is a product of superposition in our case. The lens is detected in the NVSS and FIRST surveys with an integrated flux density at 20cm of 4.8 and 5.4mJy respectively. Assuming a radio spectrum of the form $S_\nu \propto \nu^\alpha$ ($\alpha = -0.7$) the

monochromatic radio power is 3.2×10^{24} W Hz^{-1} similar to the radio galaxies studied at $z \sim 0.7$ in the 2SLAQ luminous red galaxy survey (Sadler et al. 2006). Of course, we have assumed that all of the radio flux comes from the lens. In the nearby Universe such powerful radio sources are associated with active galactic nuclei rather than star-forming galaxies.

The r-band absolute magnitude of the lens is -23.45 at $z = 0$. This assumes the SDSS r-band model magnitude of r=19.00, together with the standard cosmology, a k correction of $-0^m.87$, and the passive evolution model of $+0^m.38$ (Bernardi et al. 2003). This puts the lens in the brightest bin for LRGs. The high luminosity is also indicated by the red color (g–$i > 2.6$) of the galaxy. Color and luminosity also correlate with velocity dispersion and mass (Figures 4 and 7 of Bernardi et al. 2003). All these measurements support the idea that the lensing galaxy is a very massive object.

Let us model the lens as a singular isothermal sphere galaxy with a velocity dispersion $\sigma_v = 430$ km s^{-1}. For a lens redshift of 0.44 and a source redshift of 2.38, the deflection due to an isothermal sphere is $\sim 3.7''$. As the LRG is so massive, it provides most of the deflection needed. In physical units, the ring radius is at a projected distance of ~ 30 kpc from the center of the LRG. The (cylindrical) mass enclosed within the Einstein ring is $\sim 5.4 \times 10^{12}$ M$_\odot$. The magnification can be estimated assuming that the source size is $\sim 0''.4$ (Law et al. 2007). The ratio of the area subtended by the ring to that subtended by the source is $\sim 4R/\delta r$, where R is the ring radius and δr is the source size which is roughly same as the ring thickness. This gives a magnification of ~ 50. Though the lens galaxy provides most of the deflection, there is probably a modest contribution from the environment. Kochanek et al. (2001) showed that the ellipticity of an Einstein ring is proportional to the external shear. The Cosmic Horseshoe is nearly a perfect circle. Any contribution from the galaxy group must therefore be modest. This is surprising, as all other large separation lenses have a significant contribution from the environment.

The ring has at least four density knots, whose locations are noted in Section 2. A more sophisticated algorithm that fits to the image locations and relative brightnesses is provided by the method of Evans & Witt (2003). Here, the lens density has an isothermal profile in radius, but the angular shape of the isodensity contours is given by a Fourier series. Fermat surfaces and critical curves are presented for two possible models in Figure 5. In the left panel, the positive parity images are A and C, whilst the negative parity images corresponding to saddle-points on the Fermat surface and are B and D. In the right panel, C is regarded as a merging pair (C$_1$ and C$_2$), whilst A and D are retained as images and B is discarded. In both cases, the mass enclosed within the Einstein ring is $\sim 6 \times 10^{12}$ M$_\odot$, similar to our crude estimates, while the magnification is in the range $25 - 35$. Also possible is that the Cosmic Horseshoe is a sextuplet system, with C a conglomeration of three merging images in addition to A,B and D (see e.g., Evans & Witt 2001).

The combination of high absolute luminosity and large magnification factor makes the Cosmic Horseshoe the brightest galaxy known at $z > 2$. The lens galaxy is

one of the most massive LRGs ever detected. Detailed studies of this remarkable system at a variety of wavelengths, from optical to sub-mm will help us probe the physical nature of star formation in the young universe, whilst detailed modeling will enable us to study the interplay between baryons and dark matter in very massive galaxies.

REFERENCES

Afanasiev V. L., Moiseev A. V., 2005, AstL, 31, 194 (astro-ph/0502095)

Allam, S. S., Tucker, D. L., Lin, H., Diehl, H. T., Annis, J., Buckley-Geer, E. J., & Frieman, J. A. 2007, ApJ, 662, L51

Bernardi, M., et al. 2003, AJ, 125, 1849

Bernardi, M., et al. 2006, AJ, 131, 2018

Bolton, A. S., Burles, S., Koopmans, L. V. E., Treu, T., & Moustakas, L. A. 2006, ApJ, 638, 703

Cabanac, R. A., Valls-Gabaud, D., Jaunsen, A. O., Lidman, C., & Jerjen, H. 2005, A&A, 436, L21

Calzetti, D., Armus, L., Bohlin, R. C., Kinney, A. L., Koorneef, J., & Storchi-Bergmann, T. 2000, ApJ, 533, 682

Chandar, R., Leitherer, C., Tremonti, C. A., Calzetti, D., Aloisi, A., Meurer, G. R., & de Mello, D. 2005, ApJ, 628, 210

Erb, D. K., Shapley, A. E., Pettini, M., Steidel, C. C., Reddy, N. A., & Adelberger, K. L. 2006a, ApJ, 644, 813.

Erb, D. K., Steidel, C. C., Shapley, A. E., Pettini, M., Reddy, N. A., & Adelberger, K. L. 2006b, ApJ, 646, 107.

Evans, N. W., & Witt, H. J. 2001, MNRAS, 327, 1260

Evans, N. W., & Witt, H. J. 2003, MNRAS, 345, 1351

Inada, N., et al. 2003, Nature, 426, 810

Inada, N., et al. 2003, AJ, 126, 666

Irwin, M.J., Lewis, J.R., 2001, New Ast Rev, 45, 105

Johnston, D. E., et al. 2003, AJ, 126, 2281

King, L. J., et al. 1998, MNRAS, 295, L41

Kochanek, C. S., Keeton, C. R., & McLeod, B. A. 2001, ApJ, 547, 50

Law, D. R., Steidel, C. C., Erb, D. K., Pettini, M., Reddy, N. A., Shapley, A. E., Adelberger, K. L., & Simenc, D. J. 2007, ApJ, 656, 1

Leitherer, C. et al. 1999, ApJS, 123, 3

Miralda-Escude, J., & Lehar, J. 1992, MNRAS, 259, 31P

Morgan, N. D., Snyder, J. A., & Reens, L. H. 2003, AJ, 126, 2145

Oguri, M. 2006, MNRAS, 367, 1241

Reddy, N. A., Steidel, C. C., Pettini, M., Adelberger, K. L., Shapley, A. E., Erb, D. K., & Dickinson, M. 2007, ApJ, in press.

Sadler, E. et al. 2006, MNRAS, in press (astro-ph/0612019)

Shapley A. E., Steidel C. C., Pettini M., Adelberger K. L., 2003, ApJ, 588, 65

Steidel, C. C., Shapley, A. E., Pettini, M., Adelberger, K. L., Erb, D. K., Reddy, N. A., & Hunt, M. P. 2004, ApJ, 604, 534

Warren, S. J., Hewett, P. C., Lewis, G. F., Moller, P., Iovino, A., & Shaver, P. A. 1996, MNRAS, 278, 139

Willis, J. P., Hewett, P. C., & Warren, S. J. 2005, MNRAS, 363, 1369

TABLE 1
Properties of the Cosmic Horseshoe

Component	Parameter	
Lens	Right ascension	11:48:33.15
	Declination	19:30:03.5
	Redshift, z_L	0.444
	Magnitudes (SDSS), g_L, r_L, i_L	$20\overset{m}{.}8$, $19\overset{m}{.}0$, $18\overset{m}{.}2$
	Effective radii (INT), $R_{\mathrm{eff},g}$, $R_{\mathrm{eff},i}$	$2.2''$, $1.7''$
	Axis ratio (INT, in g,i)	0.8, 0.9
	Position angle (INT, in g,i)	$99°$, $95°$
	Radio Flux (FIRST,NVSS)	5.4 mJy, 4.8 mJy
Source	Redshift, z_S	2.379
Ring	Diameter	$10\overset{''}{.}2$
	Length	$300°$
	Total magnitudes (INT) u, g, i	$21\overset{m}{.}6$, $20\overset{m}{.}1$, $19\overset{m}{.}7$
	Mass Enclosed	5.4×10^{12} M$_\odot$